O-GlcNAcylation promotes YTHDF1 cytosolic localization and colorectal cancer tumorigenesis

Jie Li[1,*], Muhammad Ahmad[1,*], Lei Sang[2,*], Yahui Zhan[1,*], Yibo Wang[3], Yonghong Yan[4], Yue Liu[1], Weixiao Mi[1], Mei Lu[2], Yu Dai[5], Rou Zhang[6], Meng-Qiu Dong[4], Yun-Gui Yang[7], Xiaohui Wang[3,8,§], Jianwei Sun[2,§], and Jing Li [1,§]

[1]Beijing Key Laboratory of DNA Damage Response and College of Life Sciences, Capital Normal University, Beijing 100048, China

[2]Center for Life Sciences, School of Life Sciences, State Key Laboratory for Conservation and Utilization of Bio-Resources in Yunnan, Yunnan University, Kunming 650091, China

[3]Laboratory of Chemical Biology, Changchun Institute of Applied Chemistry, Chinese Academy of Sciences, Changchun, 130022, China

[4]National Institute of Biological Sciences, Beijing 102206, China

[5]Department of Stomatology, Shenzhen Peoples Hospital, the Second Clinical Medical College, Jinan University; the First Affiliated Hospital, Southern University of Science and Technology, Shenzhen, Guangdong 518020, China

[6]School of Pharmaceutical Sciences, Sun Yat-sen University, Guangzhou, Guangdong 510006, China;

[7] CAS Key Laboratory of Genomic and Precision Medicine, Collaborative Innovation Center of Genetics and Development, College of Future Technology, Beijing Institute of Genomics, Chinese Academy of Sciences, Beijing 100101, China; University of Chinese Academy of Sciences, Beijing 100049, China; Institute of Stem Cell and Regeneration, Chinese Academy of Sciences, Beijing 100101, China

[8]School of Applied Chemistry and Engineering, University of Science and Technology of China, Hefei, Anhui 230026, China

Running title: O-GlcNAcylation of YTHDF1

[*]These authors contributed equally to this work.

[§]To whom correspondence should be addressed:
Jing Li, Beijing Key Laboratory of DNA Damage Response and College of Life

Sciences, Capital Normal University, Beijing 100048, China
Phone:86-10-68901692**,** E-mail: jing_li@mail.cnu.edu.cn
Jianwei Sun, Center for Life Sciences, School of Life Sciences, State Key Laboratory for Conservation and Utilization of Bio-Resources in Yunnan, Yunnan University, Kunming 650091, China, E-mail: jwsun@ynu.edu.cn
Xiaohui Wang, Laboratory of Chemical Biology, Changchun Institute of Applied Chemistry, Chinese Academy of Sciences, Changchun, 130022, China, E-mail: xiaohui.wang@ciac.ac.cn

Abstract

O-linked N-acetylglucosamine (O-GlcNAc) is an emerging post-translation modification that couples metabolism with cellular signal transduction by crosstalking with phosphorylation and ubiquitination to orchestrate various biological processes. Herein we show that it modifies the N^6-methyladenosine (m^6A)-mRNA reader YTHDF1 and fine-tunes its nuclear translocation by the exportin protein Crm1. First we present evidence that YTHDF1 interacts with the sole O-GlcNAc transferase (OGT). Second, we verified the YTHDF1 O-GlcNAcylation sites to be Ser196/Ser197/Ser198, as described in previous numerous chemoproteomic studies. Then we constructed the O-GlcNAc-deficient YTHDF1-S196AS197FS198A (AFA) mutants, which significantly attentuated O-GlcNAc signals. Moreover, we revealed that YTHDF1 is a nucleocytoplasmic protein, whose nuclear export is mediated by Crm1. Furthermore, O-GlcNAcylation increases the cytosolic portion of YTHDF1 by enhancing binding with Crm1, thus upregulating the downstream target (e.g. c-Myc) expression. Molecular dynamics simulations suggest that O-GlcNAcylation at S197 might promote the binding between the nuclear export signal motif and Crm1 through increasing hydrogen bonding. Mouse xenograft assays further demonstrate that YTHDF1-AFA mutants decreased the colon cancer mass and size via decreasing c-Myc expression. In sum, we found that YTHDF1 is a nucleocytoplasmic protein, whose cytosolic localization is dependent on O-GlcNAc modification. We propose that the OGT-YTHDF1-c-Myc axis might underlie colorectal cancer tumorigenesis.

Key words： O-GlcNAc, YTHDF1, Crm1, m^6A, c-myc

Introduction

The N^6-methyladenosine (m^6A) modification is quite abundant on internal mRNAs and its function and regulation has caught a wave of intense investigations (1,2). Its numerous writers, erasers and readers are under stringent control (3), and one of the readers is YTH domain family 1 (YTHDF1) (4). YTHDF1 promotes translation efficiency during arsenite recovery (5). YTHDF1 enhances translation in adult mouse dorsal root ganglions during injury recovery and augments axonal regeneration (6). YTHDF1 fuels translation upon neuronal stimuli, which is conducive to learning and memory (7). YTHDF1 also recognizes m^6A-marked lysosomal protease mRNAs, thus mediating the decay of neoantigens and bolstering tumor suppressive immunotherapy(8). Recently, YTHDF1 and YTHDF3 are also found to promote stress granule formation, as m^6A mRNAs are found to be enriched in stress granules (9).

The interconnection between m^6A mRNA and cancer are being revealed (10-12), as m^6A takes part in many aspects of tumor biology: cancer stem cell, tumor cell proliferation or oncogene expression. YTHDF1, in particular, has been found to be at the nexus of multiple tumorigenic pathways. YTHDF1 binds the m^6A modified mRNA of c-Myc, whose enhanced translation would promote glycolysis and cancer cell proliferation (13). In non-small cell lung cancer, YTHDF1 upregulates the translation efficiency of CDK2, CDK cyclin D1, and YTHDF1 is also elevated in high-altitude people, possibly through the hypoxia Keap1-Nrf2-AKR1C1 pathway (14). In gastric cancer, YTHDF1 enhances the expression of frizzled 7 (FZD7), a key Wnt receptor that would hyper-activate the Wnt/β-catenin pathway (15). In ovarian

cancer, YTHDF1 promotes the translation of Eukaryotic Translation Initiation Factor 3 Subunit C (EIF3C), a component of the protein translation initiation factor EIF3 complex (16). In cervical cancer, YTHDF1 elevates the translation of hexokinase 2 (HK2) via binding with its 3'-UTR, thus promoting the Warburg effect (17). All these results suggest that YTHDF1 binds with its targets via m^6A mRNA, and plays a fundamental role during human carcinogenesis.

Investigations show that some of the m^6A regulators are subject to post-translational modifications (PTMs). YTHDF2, another m^6A reader that mediates mRNA decay (18), is subject to SUMOylation at K571 upon hypoxia stress (19). SUMOylation would alter the binding affinity of YTHDF2 with m^6A, thus deregulating the downstream target genes, leading to lung cancer progression (19). An m^6A writer, Methyltransferase-like 3 (METTL3), is modified by lactylation at its zinc-finger domain, which changes its RNA capturing capacity, and regulates immunosuppression of tumor-infiltrating myeloid cells (20). Mettl3 is also acetylated, which regulates its localization and cancer metastasis (21).

The O-linked N-acetylglucosamine (O-GlcNAc) glycosylation is one PTM that occurs intracellularly (22) (23). Functioning as a rheostat to environmental stress or cellular nutrient status, O-GlcNAc monitors transcription, neural development, cell cycle and stress response (22) (23). However, whether it plays a role in m^6A regulation has remained enigmatic. Historically O-GlcNAc studies have been strenuous due to technical impediment. Recent years have witnessed the combined methodology of chemoenzymatic labeling, bioorthogonal conjugation and ETD mass spectrometry,

which have smoothened the way for biological investigations. Previously, an isotope-tagged cleavable linker together with chemoenzymatic labeling screen has identified the O-GlcNAc sites of YTHDF1 to be S196 and S198 (24). A second enrichment strategy using Gal labeling followed by chemical oxidation points the YTHDF1 O-GlcNAcylation region to be Ser196-198 (25). In another isotope targeted glycoproteomic study in T cells, YTHDF1 O-GlcNAcyation occurs on several residues, including Ser196, Ser197 and Ser198 (26). In this manuscript, we first confirmed that YTHDF1 O-GlcNAcylation occurs on Ser196Ser197Ser198. Then we found that YTHDF1 is a nucleocytoplasmic protein with exportin 1 (CRM1) mediating its cytoplasmic shuttling. We further presented evidence that O-GlcNAcylation promotes YTHDF1 cytosolic localization, thus enhancing downstream target expression, such as c-Myc. Our results were further correlated with TCGA analysis combined with mouse xenograft models. Our data highlight the signification of glycosylation in m^6A regulation and tumorigenesis.

Results

YTHDF1 is O-GlcNAcylated at Ser196 Ser197 Ser198

As YTHDF1 has reproducibly been identified in O-GlcNAc profiling screens (27-29), we first assessed the binding affinity between YTHDF1 and the sole O-GlcNAc writer-OGT. 293T cells were transfected with Flag-YTHDF1 and HA-OGT plasmids, and the two overproduced proteins coimmunoprecipitate (coIP) (Fig. 1A). When the endogenous proteins were examined, YTHDF1 proteins were

also present in the anti-OGT immunoprecipitates (Fig. 1B). Then pulldown assays were utilized to evaluate the physical association. 293T cells were transfected with HA-OGT, and the cell lysates were incubated with recombinant GST-YTHDF1 proteins. GST-YTHDF1 pulled-down overproduced OGT proteins (Fig. 1C). When pulldown assays were carried out between recombinant OGT and YTHDF1, again GST-YTHDF1 pulled-down His-OGT (Fig. 1D), suggesting that OGT and YTHDF1 directly interact *in vivo* and *in vitro*.

Then we assessed the O-GlcNAcylation of YTHDF1. 293T cells were enriched for O-GlcNAc by supplementing the media with glucose and Thiamet-G (TMG, the OGA inhibitor) (TMG + Glu) as previously described (30,31). The endogenous YTHDF1 proteins were IPed from the lysates, and RL2 antibodies detected a crisp band upon O-GlcNAc enrichment (Fig. 1E), suggesting that YTHDF1 is indeed O-GlcNAcylated. We decided to mutate the three Ser, as several chemoproteomic studies have identified YTHDF1 O-GlcNAcylation sites to be Ser196-198 (27-29). Thus we generated a YTHDF1-S196AS197FS198A (AFA) mutant. When we transfected the WT and AFA mutant into cells, the AFA mutant significantly diminished YTHDF1 O-GlcNAcylation levels (Fig. 1F), suggesting that they are the main glycosylation sites.

Crm1 mediates the nuclearcytoplasmic shuttling of YTHDF1

To investigate the potential YTHDF1 O-GlcNAcylation functions, we first employed an immunoprecipitation-mass spectrometry (MS) analysis. Flag-YTHDF1

plasmids were transfected into cells and the lysates were immunoprecipitated with anti-Flag antibodies. Interestingly, the MS results revealed many importins and exportins (data not shown). When we did literature research, YTHDF1 was among the binding partners of exportin 1 (Crm1) in a recent proteomic study (32). Therefore, we suspect that YTHDF1 might be a nuclearcytoplasmic protein and Crm1 might mediat the process.

To test this possibility, we first assessed the association between YTHDF1 and Crm1. We also utilized KPT-330, a Crm1 inhibitor. Overexpressed YTHDF1 coIPs with Crm1, and KPT-3301 markedly reduced the interaction (Fig. 2A). Moreover, endogenous YTHDF1 interacts with Crm1 (Fig. 2B), suggesting that YTHDF1 could be a nuclearcytoplasmic protein. We then utilized the nuclear cytoplasmic fractionation assay, and fractionation results revealed that there is indeed a nuclear portion of YTHDF1 (Fig. 2C). We further adopted KPT-330 in the fractionation assay and found that KPT-330 significantly enhanced the nuclear fraction of YTHDF1 (Fig. 2D). Furthermore, in immunofluorescence staining samples, both endogeous YTHDF1 and overproduced YTHDF1 manifested significant upregulation of nuclear staining signals (Fig. 2E-F), suggesting that Crm1 could export YTHDF1 to the cytosol.

YTHDF1 O-GlcNAcylation promotes interaction with Crm1

To determine if O-GlcNAcylation plays a role in Crm1-mediated YTHDF1 nuclear shuttling, we enriched for protein O-GlcNAcylation by TMG + Glu as

previously described (30). We found that O-GlcNAc enrichment increased the binding between YTHDF1 and Crm1 (Fig. 3A). We also repressed O-GlcNAcylation by an OGT inhibitor, Acetyl-5S-GlcNAc (5S-G) (33). 5S-G treatment significantly reduced the affinity between YTHDF1 and Crm1 (Fig. 3B). When 5S-G was included in the fractionation assay, the nuclear YTHDF1 is upregulated notably (Fig. 5C), suggesting that O-GlcNAcylation increases the binding between YTHDF1 and Crm1.

Then we directly measured the effect using the AFA mutant. YTHDF1-AFA displayed marked reduction in association with Crm1 (Fig. 3D). And in the fractionation analysis, AFA again manifested much higher portion in the nucleus (Fig. 3E). Lastly, we employed fluorescent microscopy to visualize whether O-GlcNAcylation could affect YTHDF1 localization. As shown in Figure 3F-G, both 5S-G treatment and the AFA mutant enhanced nuclear YTHDF1 staining, probably by blocking its nuclear export via Crm1. These assays suggest that YTHDF1 O-GlcNAcylation promotes the binding between YTHDF1 and Crm1 and the resultant nuclear export.

A potential Nuclear Export Signal (NES) lies in proximity to YTHDF1 O-GlcNAcylation sites

We are curious why O-GlcNAcylation has such a conspicuous effect on YTHDF1 localization and looked for potential nuclear export signals (NES) surrounding the S196S197S198 region. As NES consists of the Φ1-X(2-3)-Φ2-X(2-3)-Φ3-X-Φ4 motif (Φ: hydrophobic amino acid) (34), we found a potential NES justaposing the

196-198 Ser cluster (Fig. 4A). We mutated the corresponding hydrophobic amino acid to Ala and generated 4A (Fig. 4A), as previously described for the NES of the cyclic GMP-AMP (cGAMP) synthase (cGAS) (35). When we examined for YTHDF1-Crm1 association, the 4A mutant significantly downregulated the binding with Crm1 (Fig. 4B). In the fractionation studies, 4A also elevated nuclear YTHDF1 localization (Fig. 4C). In the immunofluorescent staining experiments, 4A also has a more prominent nuclear localization pattern compared to the control (Fig. 4D). Combined, these data suggest that O-GlcNAcylation might boost the association of the neighbouring NES with Crm1.

Molecular dynamics (MD) simulations suggest that S197 O-GlcNAcylation increases the interaction between NES and Crm1 via hydrogen bonds.

We then explored deeper as why O-GlcNAcylation increases binding with Crm1. Recently a structural study focusing on the interface between NES and CRM1 found that many NESs might form hydrogen bonds with CRM1 (36), therefore we wondered whether hydrophilic O-GlcNAc could enhance the interaction by increasing hydrogen bonding. And we utilized the molecular dynamics (MD) simulation approach and began by constructing the system. Since the AlphaFold Protein Structure Database cannot well predict the NES domain of YTHDF1 (pLDDT < 50)(37,38), the ColabFold web server was used to build the initial structure of a short fragment (residues 182 - 210) including the NES domain (Fig. 5A)(39). The initial structure was further optimized for 300 ns with molecular dynamics simulations (Fig. 5B and C). The binding domain of CRM1 (residues 362

– 645, Fig.5D) was cropped from the crystal structure of the PKI NES-CRM1-RanGTP nuclear export complex (PDB ID: 3NBY)(40). The Rosetta Docking protocol (version 3.12) was applied to build the YTHDF1 NES and CRM1 complex (41-43). The NES fragment was set as the input structure with 10 Å translation and 360° rotation. One hundred poses were created after the docking process (Fig. 5E) and only two obtained reasonable relative positions (the NES domain is close to the CRM1 binding domain) (Fig. 5F). After 500 ns of MD simulations, only one complex maintained a reasonable interaction (Fig. 5G). The last frame of this complex was chosen as the initial structure for further analysis.

The root-mean-square deviation (RMSD) values indicated that both systems can reach stable states in 200 ns (Fig. 5H). The trajectory of the last 100 ns was extracted for further analysis. The binding energy of glycosylated fragment to CRM1 binding domain was -118.04 ± 0.32 kcal/mol, which is lower than that of the unglycosylated fragment to the CRM1 binding domain (-116.21 ± 0.24 kcal/mol) (Fig. 5I). The number of hydrogen bonds between the fragment and CRM1 was increased when S197 was glycosylated (3.70 ± 0.06 in the glycosylated system vs. 3.32 ± 0.04 in the non-glycosylated system, Fig. 5J) because the glycan at S197 can frequently form hydrogen bonds with H577 and D535 in CRM1 to pull the NES domain to the CRM1 binding domain (Fig. 5K). Taken together, MD simulations suggest that O-GlcNAc might increase hydrogen bonding between YTHDF1 and Crm1.

YTHDF1 O-GlcNAcylation promotes downstream target expression (e.g. c-Myc)

Recently, many YTHDF1-mediated m^6A mRNA targets have been identified, such as the protein translation initiation factor EIF3 (16), the key Wnt receptor

frizzled7 (FZD7) (15) and c-Myc (13). We focused on c-Myc, as m^6A-modified c-Myc mRNA has been demonstrated to recruit YTHDF1 (13). We reasoned that YTHDF1 O-GlcNAcylation would promote c-Myc expression as there is more cytosolic YTHDF1. We first carried out a TCGA analysis, and found that in colon adenocarcinoma (COAD) and rectum adenocarcinoma (READ) samples, both YTHDF1 and c-Myc are overexpressed in the tumor samples (Fig. 5A-B), indicative of a positive correlation between YTHDF1 and c-Myc in colorectal cancer. We therefore generated stable YTHDF1-knockdown SW620 cells using sh*YTHDF1*, and indeed c-Myc protein levels are attenuated upon YTHDF1 downregulation (Fig. 5C). When the knockdown cells were rescued with YTHDF1-WT or -AFA plasmids, c-Myc expression is comparable to the control in the YTHDF1-WT rescued cells, but not in the -AFA rescued cells (Fig. 5D). The stable SW620 cells were then utilized in mouse xenograft experiments, and the tumor size and weight were monitored (Fig. 5E-G). As expected, the YTHDF1-WT rescued cells produced much larger tumors compared to the AFA mutants, suggesting that YTHDF1 O-GlcNAcylation promotes colorectal cancer, probably via c-Myc.

Discussion

In this work, we first confirmed that YTHDF1 O-GlcNAcylation occurs on Ser196/197/198, then we identified that glycosylation promotes shuttling of YTHDF1 to the cytoplasm by CRM1. Consequently, cytosolic YTHDF1 will upregulate its downstream target expression (e.g., c-Myc), and then tumorigenesis will ensue.

Our work is in line with the observation that O-GlcNAcylation elevation correlates with different cancer types, such as breast cancer, prostate cancer, bladder cancer (44). In colon cancer, both O-GlcNAc and OGT abundance increased in clinical patient samples (45). Here we found that YTHDF1 O-GlcNAcylation boost the expression of c-Myc, at least in SW620 cells. In xenograft models, the O-GlcNAc-deficient YTHDF1-AFA mutants attenuated tumor progression, suggesting that OGT could regulate many more downstream substrates to promote cancer growth.

Of the many m^6A readers, YTHDF1-3 have been considered as cytosolic proteins (46). We show here that YTHDF1 is partly localized to the nucleus, and we found a potential NES in YTHDF1. Incidentally, the NES neighbors the O-GlcNAcylation sites, suggesting that O-GlcNAcylation might promote the interaction between NES and Crm1. MD simulations suggest that the hydrophilic O-GlcNAcylation might increase the binding between NES and Crm1 through hydrogen bonding.

A great many investigations have shown that O-GlcNAcylation alters protein localization, such as pyruvate kinase M2 (PKM2) (47) and serine/arginine-rich protein kinase 2 (SRPK2) (48). PKM2 O-GlcNAcylation at Thr405/Ser406 promotes ERK-dependent phosphorylation of PKM2 at Ser37, which is required for PKM2 nuclear translocation (47,49). And PKM2-T405A/S406A attenuates interaction with importin α5(47). SRSF Protein Kinase 2 (SRPK2) is O-GlcNAcylated at Ser490/Thr492/Thr498, which is close to a nuclear localization signal (NLS) (48). And this NLS mediates SRPK2 nuclear localization by importin α (48). Indeed, a

general mechanism has been proposed that at least some O-GlcNAcylated proteins are imported to the nucleus by importin α (48). Our work here suggest that maybe in some other cases, O-GlcNAcylation might shuttle the O-GlcNAcylated proteins to the cytoplasm by exportin.

The intertwined relationship between RNA and glycosylation is just emerging. Recently, a "glycoRNA"concept has been coined as small noncoding RNAs are found to be decorated with sialylated glycans (50). As far as m^6A is concerned, many readers have been identified in O-GlcNAc chemoproteomic profiling works (25,26,29,51,52), including YTHDF1, YTHDF3 and YTHDC1. In a recent investigation from our group (https://doi.org/10.1101/2022.09.03.506498), we found that YTHDC1 O-GlcNAcylation is induced upon DNA damage and takes part in homologous recombination by enhancing binding with m^6A mRNA. Here we show that YTHDF1 O-GlcNAcylation mediates its localization by promoting binding with exportin. We think that O-GlcNAcylation is bound to be found in many more aspects of RNA metabolism, as sweetness lies in the heart of our fellow glycobiologists.

Materials and methods

Cell culture, antibodies and plasmids

Cells were purchased from ATCC. OGT plasmids and antibodies were described before(53). Antibodies: YTHDF1 (Proteintech, #17479-1-AP), c-Myc (Abcam, Ab32072), Lamin A/C (CST, 2032S). YTHDF1 shRNA sequences (TRCN0000286871):

5’-CCGGCCCGAAAGAGTTTGAGTGGAACTCGAGTTCCACTCAAACTCTTTC GGGTTTTTG-3’

Immunoprecipitation (IP) and Immunoblotting (IB) assays

IP and IB experiments were performed as described before (54). Nuclear and cytoplasmic fractionation assays were carried out as before (55). The following primary antibodies were used for IB: anti-β-actin (1:10000), anti-HA (1:1000), and anti-FLAG M2 (Sigma) (1:1000), anti-Myc (1:1000), anti-YTHDF1 (1:1000), Lamin A/C (1:1000). Peroxidase-conjugated secondary antibodies were from JacksonImmuno Research. Blotted proteins were visualized using the ECL detection system (Amersham). Signals were detected by a LAS-4000, and quantitatively analyzed by densitometry using the Multi Gauge software (Fujifilm). All western blots were repeated for at least three times.

Cell Culture Treatment

Chemical utilization: Thiamet-G (TMG) (OGA inhibitor) at 5 μM for 24 hrs; acetyl-5S-GlcNAc (5S-G) (OGT inhibitor) was used at 100 μM (prepared at 50 mM in DMSO) for 24 hrs; KPT-300 (Crm1 inhibitor) at 5 μM for 24 hrs.

Indirect Immunofluorescence

Indirect immunofluorescence staining was performed as described before (54). Dilutions of primary antibodies were 1:500 for mouse anti-YTHDF1, and 1:1000 for

anti-Flag antibodies. Cell nuclei were stained with DAPI.

Molecular Dynamics (MD) Simulations

The O-glycan (*β-N*-Acetyl-$_D$-Glucosamine) at S197 of the YTHDF1 fragment was built using the Glycan Reader & Modeler module (56). The role of O-glycosylation in the YTHDF1 fragment interacting with CRM1 was investigated via molecular dynamics simulations with the GROMACS (version 2021.2) software package(57,58). Two systems (unglycosylated fragment and O-GlcNAcylated fragment at S197 in complex with CRM1 binding domain, respectively) were neutralized and solvated by 150 mM KCl and TIP3P water molecules. The systems were minimized and equilibrated using the default equilibration inputs from the CHARMM-GUI webserver(59) with the CHARMM36m force field (60,61). In brief, the systems were equilibrated in the isothermal-isobaric (NPT) ensemble for 200 ns. The pressure was set at 1 atm maintained by the Parrinello-Rahman barostat (62) and the temperature was maintained at 310.15 K with the Nosé–Hoover thermostat(63). Periodic boundary conditions were applied throughout the simulations. The SHAKE algorithm was used to constrain all bonds with hydrogen atoms(64). The particle-mesh Ewald (PME) summation method was applied to treat long-range electrostatic interactions (65).

Analysis of MD trajectory data was performed through MDAnalysis (66). The binding energy (enthalpy) and per-residue energy contributions were calculated by the molecular mechanics/Poisson-Boltzmann (generalized-Born) surface area method with the gmx_MMPBSA tool (67,68). The interactions between the YTHDF1 fragment and the CRM1 binding domain were displayed by PyMol (69).

Mouse Xenograft

1 X 10^6 control，YTHDF1 shRNA, YTHDF1 shRNA; YTHDF1-WT or YTHDF1 shRNA;YTHDF1-AFA stable SW620 cells were resuspended in Matrigel (Corning) and then injected into the flanks of nude mice (4-6 weeks old). The tumor volumes were measured from day 3 to 9 after injection. At 9 days after the injection, tumors were dissected. The mice were obtained from the Animal Research and Resource Center, Yunnan University. {Certification NO. SCXK(Dian)K2021-0001}. All animal work procedures were approved by the Animal Care Committee of the Yunnan University (Kunming, China).

Data Availability Statement

All data are contained within the manuscript.

Abbreviation

Thiamet-G (TMG); Mass spectrometry (MS); Immunoprecipitation (IP); Immunoblotting (IB); Acetyl-5S-GlcNAc (5S-G); O-linked β-N-acetylglucosamine (O-GlcNAc); O-GlcNAc transferase (OGT); mRNA N^6-methyladenosine (m^6A); electron transfer dissociation (ETD);

Acknowledgements

We thank Dr. Xing Chen (Peking Univ.) for reagents, and Dr. Qing Chang for providing facility support at the Protein Preparation and Characterization Platform of

Tsinghua University Technology Center for Protein Research. This work was supported by the National Natural Science Foundation of China (NSFC) fund (31872720 and 32271285), R & D Program of Beijing Municipal Education Commission (KZ202210028043) to Jing L. and NSFC (82273460) fund and the Yunnan Applied Basic Research Projects (202101AV070002 and 2019FY003030) to J. S.

Conflict of interest

The authors declare that they have no conflicts of interest with the contents of this article.

References

1. Zhao, B. S., Roundtree, I. A., and He, C. (2017) Post-transcriptional gene regulation by mRNA modifications. *Nat Rev Mol Cell Biol* **18**, 31-42
2. Adhikari, S., Xiao, W., Zhao, Y. L., and Yang, Y. G. (2016) m(6)A: Signaling for mRNA splicing. *RNA Biol* **13**, 756-759
3. Wei, J., and He, C. (2021) Chromatin and transcriptional regulation by reversible RNA methylation. *Curr Opin Cell Biol* **70**, 109-115
4. Shi, H., Wei, J., and He, C. (2019) Where, When, and How: Context-Dependent Functions of RNA Methylation Writers, Readers, and Erasers. *Mol Cell* **74**, 640-650
5. Wang, X., Zhao, B. S., Roundtree, I. A., Lu, Z., Han, D., Ma, H., Weng, X., Chen, K., Shi, H., and He, C. (2015) N(6)-methyladenosine Modulates Messenger RNA Translation Efficiency. *Cell* **161**, 1388-1399
6. Weng, Y. L., Wang, X., An, R., Cassin, J., Vissers, C., Liu, Y., Liu, Y., Xu, T., Wang, X., Wong, S. Z. H., Joseph, J., Dore, L. C., Dong, Q., Zheng, W., Jin, P., Wu, H., Shen, B., Zhuang, X., He, C., Liu, K., Song, H., and Ming, G. L. (2018) Epitranscriptomic m(6)A Regulation of Axon Regeneration in the Adult Mammalian Nervous System. *Neuron* **97**, 313-325 e316
7. Shi, H., Zhang, X., Weng, Y. L., Lu, Z., Liu, Y., Lu, Z., Li, J., Hao, P., Zhang, Y., Zhang, F., Wu, Y., Delgado, J. Y., Su, Y., Patel, M. J., Cao, X., Shen, B., Huang, X., Ming, G. L., Zhuang, X., Song, H., He, C., and Zhou, T. (2018) m(6)A facilitates hippocampus-dependent learning and memory through YTHDF1. *Nature* **563**, 249-253
8. Han, D., Liu, J., Chen, C., Dong, L., Liu, Y., Chang, R., Huang, X., Liu, Y., Wang, J., Dougherty, U., Bissonnette, M. B., Shen, B., Weichselbaum, R. R., Xu, M. M., and He, C. (2019) Anti-tumour immunity controlled through mRNA m(6)A methylation and YTHDF1 in dendritic cells. *Nature*
9. Fu, Y., and Zhuang, X. (2020) m(6)A-binding YTHDF proteins promote stress granule formation. *Nat Chem Biol* **16**, 955-963
10. Han, X., Wang, M., Zhao, Y. L., Yang, Y., and Yang, Y. G. (2021) RNA methylations in human cancers. *Semin Cancer Biol* **75**, 97-115
11. He, P. C., and He, C. (2021) m(6) A RNA methylation: from mechanisms to therapeutic potential. *EMBO J* **40**, e105977
12. Liu, J., Harada, B. T., and He, C. (2019) Regulation of Gene Expression by N(6)-methyladenosine in Cancer. *Trends Cell Biol* **29**, 487-499
13. Yang, X., Shao, F., Guo, D., Wang, W., Wang, J., Zhu, R., Gao, Y., He, J., and Lu, Z. (2021) WNT/beta-catenin-suppressed FTO expression increases m(6)A of c-Myc mRNA to promote tumor cell glycolysis and tumorigenesis. *Cell Death Dis* **12**, 462
14. Shi, Y., Fan, S., Wu, M., Zuo, Z., Li, X., Jiang, L., Shen, Q., Xu, P., Zeng, L., Zhou, Y., Huang, Y., Yang, Z., Zhou, J., Gao, J., Zhou, H., Xu, S., Ji, H., Shi, P., Wu, D. D., Yang, C., and Chen, Y. (2019) YTHDF1 links hypoxia adaptation and non-small cell lung cancer progression. *Nat Commun* **10**, 4892
15. Pi, J., Wang, W., Ji, M., Wang, X., Wei, X., Jin, J., Liu, T., Qiang, J., Qi, Z.,

Li, F., Liu, Y., Ma, Y., Si, Y., Huo, Y., Gao, Y., Chen, Y., Dong, L., Su, R., Chen, J., Rao, S., Yi, P., Yu, S., Wang, F., and Yu, J. (2021) YTHDF1 Promotes Gastric Carcinogenesis by Controlling Translation of FZD7. *Cancer Res* **81**, 2651-2665

16. Liu, T., Wei, Q., Jin, J., Luo, Q., Liu, Y., Yang, Y., Cheng, C., Li, L., Pi, J., Si, Y., Xiao, H., Li, L., Rao, S., Wang, F., Yu, J., Yu, J., Zou, D., and Yi, P. (2020) The m6A reader YTHDF1 promotes ovarian cancer progression via augmenting EIF3C translation. *Nucleic Acids Res* **48**, 3816-3831
17. Wang, Q., Guo, X., Li, L., Gao, Z., Su, X., Ji, M., and Liu, J. (2020) N(6)-methyladenosine METTL3 promotes cervical cancer tumorigenesis and Warburg effect through YTHDF1/HK2 modification. *Cell Death Dis* **11**, 911
18. Wang, X., Lu, Z., Gomez, A., Hon, G. C., Yue, Y., Han, D., Fu, Y., Parisien, M., Dai, Q., Jia, G., Ren, B., Pan, T., and He, C. (2014) N6-methyladenosine-dependent regulation of messenger RNA stability. *Nature* **505**, 117-120
19. Hou, G., Zhao, X., Li, L., Yang, Q., Liu, X., Huang, C., Lu, R., Chen, R., Wang, Y., Jiang, B., and Yu, J. (2021) SUMOylation of YTHDF2 promotes mRNA degradation and cancer progression by increasing its binding affinity with m6A-modified mRNAs. *Nucleic Acids Res* **49**, 2859-2877
20. Xiong, J., He, J., Zhu, J., Pan, J., Liao, W., Ye, H., Wang, H., Song, Y., Du, Y., Cui, B., Xue, M., Zheng, W., Kong, X., Jiang, K., Ding, K., Lai, L., and Wang, Q. (2022) Lactylation-driven METTL3-mediated RNA m(6)A modification promotes immunosuppression of tumor-infiltrating myeloid cells. *Mol Cell* **82**, 1660-1677 e1610
21. Li, Y., He, X., Lu, X., Gong, Z., Li, Q., Zhang, L., Yang, R., Wu, C., Huang, J., Ding, J., He, Y., Liu, W., Chen, C., Cao, B., Zhou, D., Shi, Y., Chen, J., Wang, C., Zhang, S., Zhang, J., Ye, J., and You, H. (2022) METTL3 acetylation impedes cancer metastasis via fine-tuning its nuclear and cytosolic functions. *Nat Commun* **13**, 6350
22. Hart, G. W., Slawson, C., Ramirez-Correa, G., and Lagerlof, O. (2011) Cross talk between O-GlcNAcylation and phosphorylation: roles in signaling, transcription, and chronic disease. *Annu Rev Biochem* **80**, 825-858
23. Yang, X., and Qian, K. (2017) Protein O-GlcNAcylation: emerging mechanisms and functions. *Nat Rev Mol Cell Biol* **18**, 452-465
24. Qin, K., Zhu, Y., Qin, W., Gao, J., Shao, X., Wang, Y. L., Zhou, W., Wang, C., and Chen, X. (2018) Quantitative Profiling of Protein O-GlcNAcylation Sites by an Isotope-Tagged Cleavable Linker. *ACS Chem Biol* **13**, 1983-1989
25. Chen, Y., Qin, H., Yue, X., Zhou, J., Liu, L., Nie, Y., and Ye, M. (2021) Highly Efficient Enrichment of O-GlcNAc Glycopeptides Based on Chemical Oxidation and Reversible Hydrazide Chemistry. *Anal Chem* **93**, 16618-16627
26. Woo, C. M., Lund, P. J., Huang, A. C., Davis, M. M., Bertozzi, C. R., and Pitteri, S. J. (2018) Mapping and Quantification of Over 2000 O-linked Glycopeptides in Activated Human T Cells with Isotope-Targeted Glycoproteomics (Isotag). *Mol Cell Proteomics* **17**, 764-775

27. Qin, K., Zhu, Y., Qin, W., Gao, J., Shao, X., Wang, Y. L., Zhou, W., Wang, C., and Chen, X. (2018) Quantitative Profiling of Protein O-GlcNAcylation Sites by an Isotope-Tagged Cleavable Linker. *ACS Chem Biol*
28. Li, J., Li, Z., Duan, X., Qin, K., Dang, L., Sun, S., Cai, L., Hsieh-Wilson, L. C., Wu, L., and Yi, W. (2019) An Isotope-Coded Photocleavable Probe for Quantitative Profiling of Protein O-GlcNAcylation. *ACS Chem Biol*
29. Huo, B., Zhang, W., Zhao, X., Dong, H., Yu, Y., Wang, J., Qian, X., and Qin, W. (2018) A triarylphosphine-trimethylpiperidine reagent for the one-step derivatization and enrichment of protein post-translational modifications and identification by mass spectrometry. *Chem Commun (Camb)* **54**, 13790-13793
30. Ramakrishnan, P., Clark, P. M., Mason, D. E., Peters, E. C., Hsieh-Wilson, L. C., and Baltimore, D. (2013) Activation of the transcriptional function of the NF-kappaB protein c-Rel by O-GlcNAc glycosylation. *Sci Signal* **6**, ra75
31. Tian, J., Geng, Q., Ding, Y., Liao, J., Dong, M. Q., Xu, X., and Li, J. (2016) O-GlcNAcylation Antagonizes Phosphorylation of CDH1 (CDC20 Homologue 1). *J Biol Chem* **291**, 12136-12144
32. Kirli, K., Karaca, S., Dehne, H. J., Samwer, M., Pan, K. T., Lenz, C., Urlaub, H., and Gorlich, D. (2015) A deep proteomics perspective on CRM1-mediated nuclear export and nucleocytoplasmic partitioning. *Elife* **4**
33. Gloster, T. M., Zandberg, W. F., Heinonen, J. E., Shen, D. L., Deng, L., and Vocadlo, D. J. (2011) Hijacking a biosynthetic pathway yields a glycosyltransferase inhibitor within cells. *Nat Chem Biol* **7**, 174-181
34. Kim, Y. H., Han, M. E., and Oh, S. O. (2017) The molecular mechanism for nuclear transport and its application. *Anat Cell Biol* **50**, 77-85
35. Sun, H., Huang, Y., Mei, S., Xu, F., Liu, X., Zhao, F., Yin, L., Zhang, D., Wei, L., Wu, C., Ma, S., Wang, J., Cen, S., Liang, C., Hu, S., and Guo, F. (2021) A Nuclear Export Signal Is Required for cGAS to Sense Cytosolic DNA. *Cell Rep* **34**, 108586
36. Fung, H. Y., Fu, S. C., and Chook, Y. M. (2017) Nuclear export receptor CRM1 recognizes diverse conformations in nuclear export signals. *Elife* **6**
37. Jumper, J., Evans, R., Pritzel, A., Green, T., Figurnov, M., Ronneberger, O., Tunyasuvunakool, K., Bates, R., Zidek, A., Potapenko, A., Bridgland, A., Meyer, C., Kohl, S. A. A., Ballard, A. J., Cowie, A., Romera-Paredes, B., Nikolov, S., Jain, R., Adler, J., Back, T., Petersen, S., Reiman, D., Clancy, E., Zielinski, M., Steinegger, M., Pacholska, M., Berghammer, T., Bodenstein, S., Silver, D., Vinyals, O., Senior, A. W., Kavukcuoglu, K., Kohli, P., and Hassabis, D. (2021) Highly accurate protein structure prediction with AlphaFold. *Nature* **596**, 583-+
38. Varadi, M., Anyango, S., Deshpande, M., Nair, S., Natassia, C., Yordanova, G., Yuan, D., Stroe, O., Wood, G., Laydon, A., Zidek, A., Green, T., Tunyasuvunakool, K., Petersen, S., Jumper, J., Clancy, E., Green, R., Vora, A., Lutfi, M., Figurnov, M., Cowie, A., Hobbs, N., Kohli, P., Kleywegt, G., Birney, E., Hassabis, D., and Velankar, S. (2022) AlphaFold Protein Structure Database: massively expanding the structural coverage of protein-sequence

space with high-accuracy models. *Nucleic Acids Res* **50**, D439-D444
39. Mirdita, M., Schutze, K., Moriwaki, Y., Heo, L., Ovchinnikov, S., and Steinegger, M. (2022) ColabFold: making protein folding accessible to all. *Nat Methods* **19**, 679-+
40. Guttler, T., Madl, T., Neumann, P., Deichsel, D., Corsini, L., Monecke, T., Ficner, R., Sattler, M., and Gorlich, D. (2010) NES consensus redefined by structures of PKI-type and Rev-type nuclear export signals bound to CRM1. *Nat Struct Mol Biol* **17**, 1367-U1229
41. Gray, J. J., Moughon, S., Wang, C., Schueler-Furman, O., Kuhlman, B., Rohl, C. A., and Baker, D. (2003) Protein-protein docking with simultaneous optimization of rigid-body displacement and side-chain conformations. *J Mol Biol* **331**, 281-299
42. Wang, C., Schueler-Furman, O., and Baker, D. (2005) Improved side-chain modeling for protein-protein docking. *Protein Sci* **14**, 1328-1339
43. Chaudhury, S., Berrondo, M., Weitzner, B. D., Muthu, P., Bergman, H., and Gray, J. J. (2011) Benchmarking and Analysis of Protein Docking Performance in Rosetta v3.2. *Plos One* **6**
44. de Queiroz, R. M., Carvalho, E., and Dias, W. B. (2014) O-GlcNAcylation: The Sweet Side of the Cancer. *Front Oncol* **4**, 132
45. Mi, W., Gu, Y., Han, C., Liu, H., Fan, Q., Zhang, X., Cong, Q., and Yu, W. (2011) O-GlcNAcylation is a novel regulator of lung and colon cancer malignancy. *Biochim Biophys Acta* **1812**, 514-519
46. Liao, S., Sun, H., and Xu, C. (2018) YTH Domain: A Family of N(6)-methyladenosine (m(6)A) Readers. *Genomics Proteomics Bioinformatics* **16**, 99-107
47. Wang, Y., Liu, J., Jin, X., Zhang, D., Li, D., Hao, F., Feng, Y., Gu, S., Meng, F., Tian, M., Zheng, Y., Xin, L., Zhang, X., Han, X., Aravind, L., and Wei, M. (2017) O-GlcNAcylation destabilizes the active tetrameric PKM2 to promote the Warburg effect. *Proc Natl Acad Sci U S A* **114**, 13732-13737
48. Tan, W., Jiang, P., Zhang, W., Hu, Z., Lin, S., Chen, L., Li, Y., Peng, C., Li, Z., Sun, A., Chen, Y., Zhu, W., Xue, Y., Yao, Y., Li, X., Song, Q., He, F., Qin, W., and Pei, H. (2021) Posttranscriptional regulation of de novo lipogenesis by glucose-induced O-GlcNAcylation. *Mol Cell* **81**, 1890-1904 e1897
49. Yang, W., Zheng, Y., Xia, Y., Ji, H., Chen, X., Guo, F., Lyssiotis, C. A., Aldape, K., Cantley, L. C., and Lu, Z. (2012) ERK1/2-dependent phosphorylation and nuclear translocation of PKM2 promotes the Warburg effect. *Nat Cell Biol* **14**, 1295-1304
50. Flynn, R. A., Pedram, K., Malaker, S. A., Batista, P. J., Smith, B. A. H., Johnson, A. G., George, B. M., Majzoub, K., Villalta, P. W., Carette, J. E., and Bertozzi, C. R. (2021) Small RNAs are modified with N-glycans and displayed on the surface of living cells. *Cell* **184**, 3109-3124 e3122
51. Qin, W., Qin, K., Fan, X., Peng, L., Hong, W., Zhu, Y., Lv, P., Du, Y., Huang, R., Han, M., Cheng, B., Liu, Y., Zhou, W., Wang, C., and Chen, X. (2018) Artificial Cysteine S-Glycosylation Induced by Per-O-Acetylated Unnatural

Monosaccharides during Metabolic Glycan Labeling. *Angew Chem Int Ed Engl* **57**, 1817-1820

52. Li, J., Li, Z., Duan, X., Qin, K., Dang, L., Sun, S., Cai, L., Hsieh-Wilson, L. C., Wu, L., and Yi, W. (2019) An Isotope-Coded Photocleavable Probe for Quantitative Profiling of Protein O-GlcNAcylation. *ACS Chem Biol* **14**, 4-10
53. Li, Z., Li, X., Nai, S., Geng, Q., Liao, J., Xu, X., and Li, J. (2017) Checkpoint kinase 1-induced phosphorylation of O-linked beta-N-acetylglucosamine transferase regulates the intermediate filament network during cytokinesis. *J Biol Chem* **292**, 19548-19555
54. Li, J., Wang, J., Hou, W., Jing, Z., Tian, C., Han, Y., Liao, J., Dong, M. Q., and Xu, X. (2011) Phosphorylation of Ataxin-10 by polo-like kinase 1 is required for cytokinesis. *Cell Cycle* **10**, 2946-2958
55. Cao, X., Li, C., Xiao, S., Tang, Y., Huang, J., Zhao, S., Li, X., Li, J., Zhang, R., and Yu, W. (2017) Acetylation promotes TyrRS nuclear translocation to prevent oxidative damage. *Proc Natl Acad Sci U S A* **114**, 687-692
56. Jo, S., Song, K. C., Desaire, H., MacKerell, A. D., Jr., and Im, W. (2011) Glycan Reader: automated sugar identification and simulation preparation for carbohydrates and glycoproteins. *J Comput Chem* **32**, 3135-3141
57. Van Der Spoel, D., Lindahl, E., Hess, B., Groenhof, G., Mark, A. E., and Berendsen, H. J. (2005) GROMACS: fast, flexible, and free. *J Comput Chem* **26**, 1701-1718
58. Abraham, M. J., Murtola, T., Schulz, R., Páll, S., Smith, J. C., Hess, B., and Lindahl, E. (2015) GROMACS: High performance molecular simulations through multi-level parallelism from laptops to supercomputers. *SoftwareX* **1-2**, 19-25
59. Jo, S., Kim, T., Iyer, V. G., and Im, W. (2008) CHARMM-GUI: a web-based graphical user interface for CHARMM. *J. Comput. Chem.* ***29***, 1859-1865
60. Best, R. B., Zhu, X., Shim, J., Lopes, P. E., Mittal, J., Feig, M., and Mackerell, A. D., Jr. (2012) Optimization of the additive CHARMM all-atom protein force field targeting improved sampling of the backbone phi, psi and side-chain chi(1) and chi(2) dihedral angles. *J. Chem. Theory Comput.* ***8***, 3257-3273
61. Huang, J., Rauscher, S., Nawrocki, G., Ran, T., Feig, M., de Groot, B. L., Grubmuller, H., and MacKerell, A. D., Jr. (2017) CHARMM36m: an improved force field for folded and intrinsically disordered proteins. *Nat. Methods* ***14***, 71-73
62. Parrinello, M., and Rahman, A. (1981) Polymorphic Transitions in Single-Crystals - a New Molecular-Dynamics Method. *J Appl Phys* **52**, 7182-7190
63. Evans, D. J., and Holian, B. L. (1985) The Nose-Hoover Thermostat. *Journal of Chemical Physics* **83**, 4069-4074
64. Blum, C. A., MJB. Roli A, Sampels, M. (2008) *Hybrid Metaheuristics, An Emerging Approach to Optimization*, Springer-Verlag, Berlin Heidelberg
65. Darden, T., York, D., and Pedersen, L. (1993) Particle mesh Ewald: AnN ·

log(N) method for Ewald sums in large systems. *J. Chem. Phys.* **98**, 10089-10092

66. Michaud-Agrawal, N., Denning, E. J., Woolf, T. B., and Beckstein, O. (2011) MDAnalysis: a toolkit for the analysis of molecular dynamics simulations. *J Comput Chem* **32**, 2319-2327
67. Valdes-Tresanco, M. S., Valdes-Tresanco, M. E., Valiente, P. A., and Moreno, E. (2021) gmx_MMPBSA: A New Tool to Perform End-State Free Energy Calculations with GROMACS. *J Chem Theory Comput* **17**, 6281-6291
68. Massova, I., and Kollman, P. A. (2000) Combined molecular mechanical and continuum solvent approach (MM-PBSA/GBSA) to predict ligand binding. *Perspect Drug Discov* **18**, 113-135
69. PyMol. The PyMOL Molecular Graphics System. in *Schrödinger, LLC*

Figure legends

Fig. 1. YTHDF1 is O-GlcNAcylated at Ser196 Ser197 Ser198. (A)293T cells were transfected with Flag-YTHDF1 and HA-OGT. The cell lysates were subject to immunoprecipitation and immunoblotting with the antibodies indicated. (B) HeLa cell lysates were immunoprecipitated with anti-OGT antibodies and immunoblotted with the indicated antibodies. (C) 293T cells were transfected with HA-OGT and the cell lysates were incubated with recombinant GST-YTHDF1. (D) Recombinant His-OGT and GST-YTHDF1 proteins were incubated and subject to pulldown assays. (E) Cells were treated with the OGA inhibitor Thiamet-G (TMG) and glucose to enrich for O-GlcNAcylation as described previously (30). Then the cell lysates were immunoprecipitated with anti-YTHDF1 antibodies and immunoblotted with anti-O-GlcNAc RL2 antibodies. (F) YTHDF1-S196A, S197F, S198A, -S196 (AFA) mutants were constructed and the cells were transfected with HA-OGT together with SFB-YTHDF1-WT, and -AFA mutants. The anti-Flag immunoprecipitates were immunoblotted with RL2 antibodies.

Fig 2. Nuclear cytoplasmic shuttling of YTHDF1 is mediated by exportin 1 (Crm1). (A) Overproduced YTHDF1 interacts with Crm1. Cells were transfected with SFB-YTHDF1 and HA-CRM1, treated or untreated with KPT-330 (Crm1 inhibitor). (B) Endogenous YTHDF1 interacts with Crm1. Cell lysates were immunoprecipitated with anti-YTHDF1 antibodies. (C) Cell lysates were subject to nuclear cytoplasmic fractionation to indicate cytosolic (CYTO) and nuclear (NUC)

portions. (D) KPT-330 treatment increases nuclear YTHDF1. Cells were transfected with SFB-YTHDF1 and treated with or without KPT-330. (E-F) Indirect immunofluorescence demonstrated that KPT-330 treatment increases the nuclear localization of endogenous YTHDF1 (E) and overexpressed YTHDF1 (F). Scale bar, 10 μM. * indicates $p<0.05$; **** indicates $p<0.0001$.

Fig. 3 O-GlcNAcylation promotes the interaction between YTHDF1 and Crm1. (A) Cells were transfected with SFB-YTHDF1 and HA-CRM1 and enriched for O-GlcNAcylation by TMG plus glucose treatment (TMG + Glu) as previously described (30). And O-GlcNAcylation enhances the binding between YTHDF1 and Crm1. (B) Cells were transfected with SFB-YTHDF1 and HA-CRM1 and treated with the OGT inhibitor Acetyl-5S-GlcNAc (5S-G). And OGT inhibition downregulated the affinity between YTHDF1 and Crm1. (C) Cells were transfected with SFB-YTHDF1 and treated with 5S-G. Nuclear and cytoplasmic fractionation assays were carried out. OGT inhibition elevated nuclear YTHDF1. (D) Cells were transfected with HA-Crm1 together with SFB-YTHDF1-WT or -AFA plasmids. (E) Cells were transfected with SFB-YTHDF1-WT or -AFA mutants and subject to nuclear and cytoplasmic fractionation assays. (F-G) Cells were transfected with SFB-YTHDF1-WT (treated or untreated with 5S-G), or -AFA. The cells were then stained with anti-Flag antibodies and DAPI. Scale bar, 10 μM. * indicates $p<0.05$; *** indicates $p<0.001$.

Fig. 4. There is a potential nuclear exportin signal (NES) in proximity to O-GlcNAcylation sites. (A) Sequence alignment of the YTHDF1-WT, O-GlcNAc-deficient AFA, and the NES-deficient 4A sequences. (B) Cells were transfected with HA-Crm1, together with YTHDF1-WT and -4A plasmids. (C) Cells were transfected with SFB-YTHDF1-WT or -4A plasmids and analyzed by nuclear cytoplasmic fractionation. (D) Cells were transfected with SFB-YTHDF1 or -4A, and stained with anti-Flag antibodies and DAPI. Scale bar, 10 μM. * indicates $p<0.05$; *** indicates $p<0.001$, ns indicates non-specific.

Fig. 5. Molecular dynamics (MD) simulations suggest that S197 O-GlcNAcylation increases the interaction between NES and Crm1 via hydrogen bonds. (A) Initial structure of YTHDF1 fragment from ColabFold. The NES domain is colored in magenta and serines that could be glycosylated are colored in yellow. (B) Root-mean-square deviation (RMSD) of backbone of YTHDF1 fragments during 300 ns of MD simulation. (C) Structure of YTHDF1 fragments after optimization. (D) Structure of CRM1. The NES binding region cropped for docking is shown in cyan. (E) Docking results for CRM1 and the YTHDF1 fragment. (F). Reasonable poses (Pose 37 in cyan and Pose 97 in magenta) chosen from 100 poses. (G) Positions of YTHDF1 before and after MD simulations in Poses 37 and 97. (H) RMSDs of the backbone of CRM1 and YTHDF1 fragments in the non-glycosylated system (black for CRM1 and red for YTHDF1 fragments) and the glycosylated system (blue for CRM1 and magenta for YTHDF1 fragment) during 200 ns of MD simulations. (I) Binding energies between CRM1 and YTHDF1 fragments in the

non-glycosylated and glycosylated systems. (J) Number of hydrogen bonds per frame in the non-glycosylated and glycosylated systems. (K) Detailed interaction between glycan and key residues in CRM1. The hydrogen bonds are shown in yellow dashed lines.

Fig. 6. YTHDF1 O-GlcNAcylation promotes c-Myc expression in colorectal carcinoma. (A-B) YTHDF1 and c-Myc mRNA levels in colon adenocarcinoma (COAD) and rectum adenocarcinoma (READ) samples from The Cancer Genome Atlas (TCGA) database. (C) Stable YTHDF1-knockdown SW620 cell lines were generated and examined for c-Myc expression. (D) The cell lines in (C) were rescued with Flag-YTHDF1-WT, or -AFA plasmids. And cellular lysates were immunoblotted with antibodies indicated. (E-G) Xenografts in nude mice. The stable SW620 cells were injected into nude mice. The tumors were imaged after 8 days. E shows the tumor images, F shows the tumor size, and G shows the tumor weight. * indicates $p<0.05$. (H) A model illustrating the role of O-GlcNAc in YTHDF1 nuclear shuttling. O-GlcNAcylation of YTHDF1 at S196S197S198 will enhance the partnership between Crm1 and YTHDF1, thus promoting cytosol localization of YTHDF1 and translation of downstream target proteins, e.g., c-Myc. Such an OGT-YTHDF1-c-Myc pathway will enhance colorectal cancer.

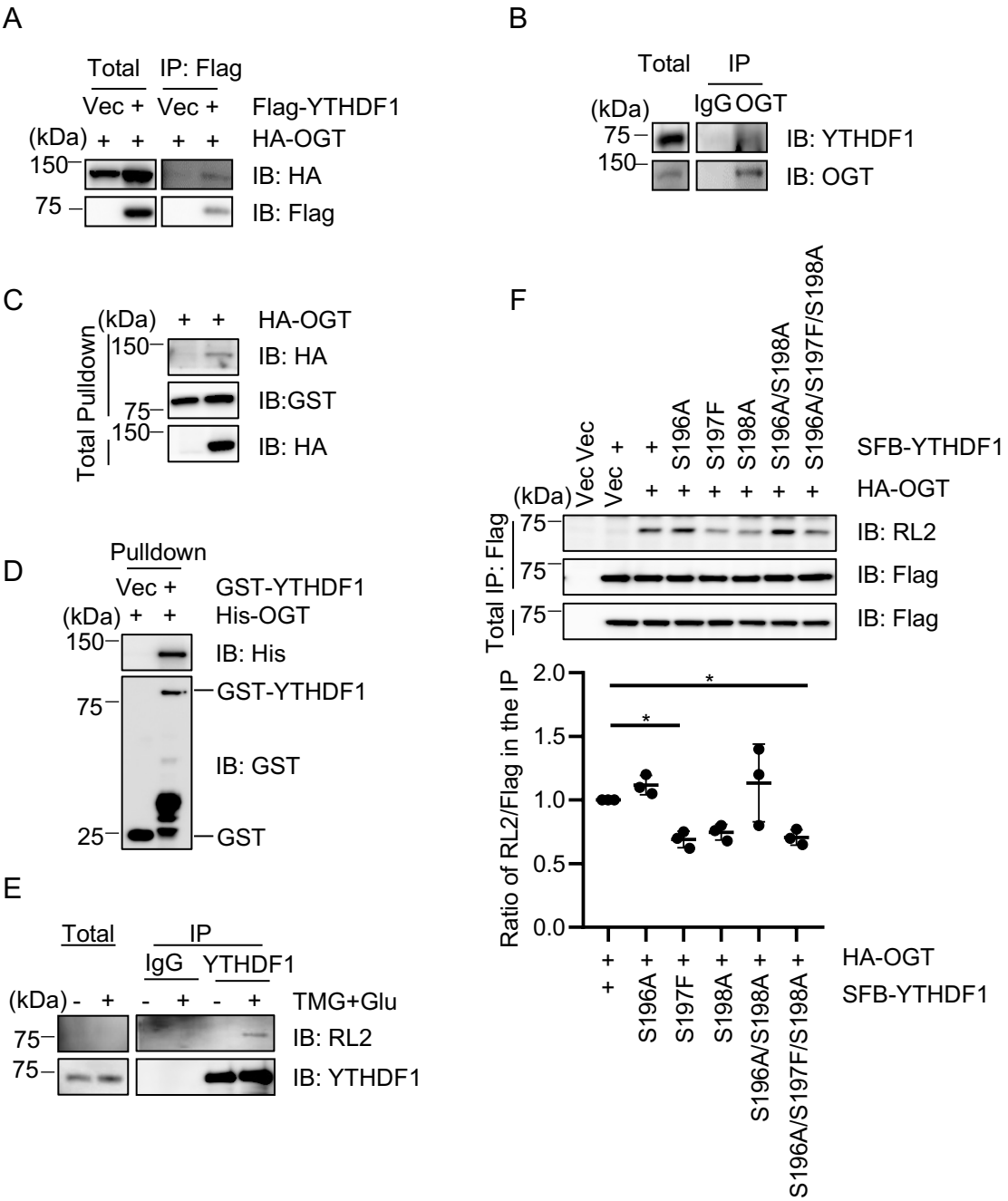
A
Total
IP: Flag
Vec +
Vec +
Flag-YTHDF1
(kDa)
+ + + +
HA-OGT
150
IB: HA
75
IB: Flag
B
Total
IP
(kDa)
IgG
OGT
75
IB: YTHDF1
150
IB: OGT
C
(kDa)
+ +
HA-OGT
Total Pulldown
150
IB: HA
75
IB:GST
150
IB: HA
D
Pulldown
Vec +
GST-YTHDF1
(kDa)
+ +
His-OGT
150
IB: His
75
GST-YTHDF1
IB: GST
25
GST
E
Total
IP
IgG
YTHDF1
(kDa)
- + - + - +
TMG+Glu
75
IB: RL2
75
IB: YTHDF1
F
Vec
Vec
Vec +
+
S196A
S197F
S198A
S196A/S198A
S196A/S197F/S198A
SFB-YTHDF1
(kDa)
+ + + + + +
HA-OGT
Total IP: Flag
75
IB: RL2
75
IB: Flag
75
IB: Flag
Ratio of RL2/Flag in the IP
2.0
1.5
1.0
0.5
0.0
*
*
+ + + + + +
HA-OGT
+ S196A S197F S198A S196A/S198A S196A/S197F/S198A
SFB-YTHDF1

Fig. 1

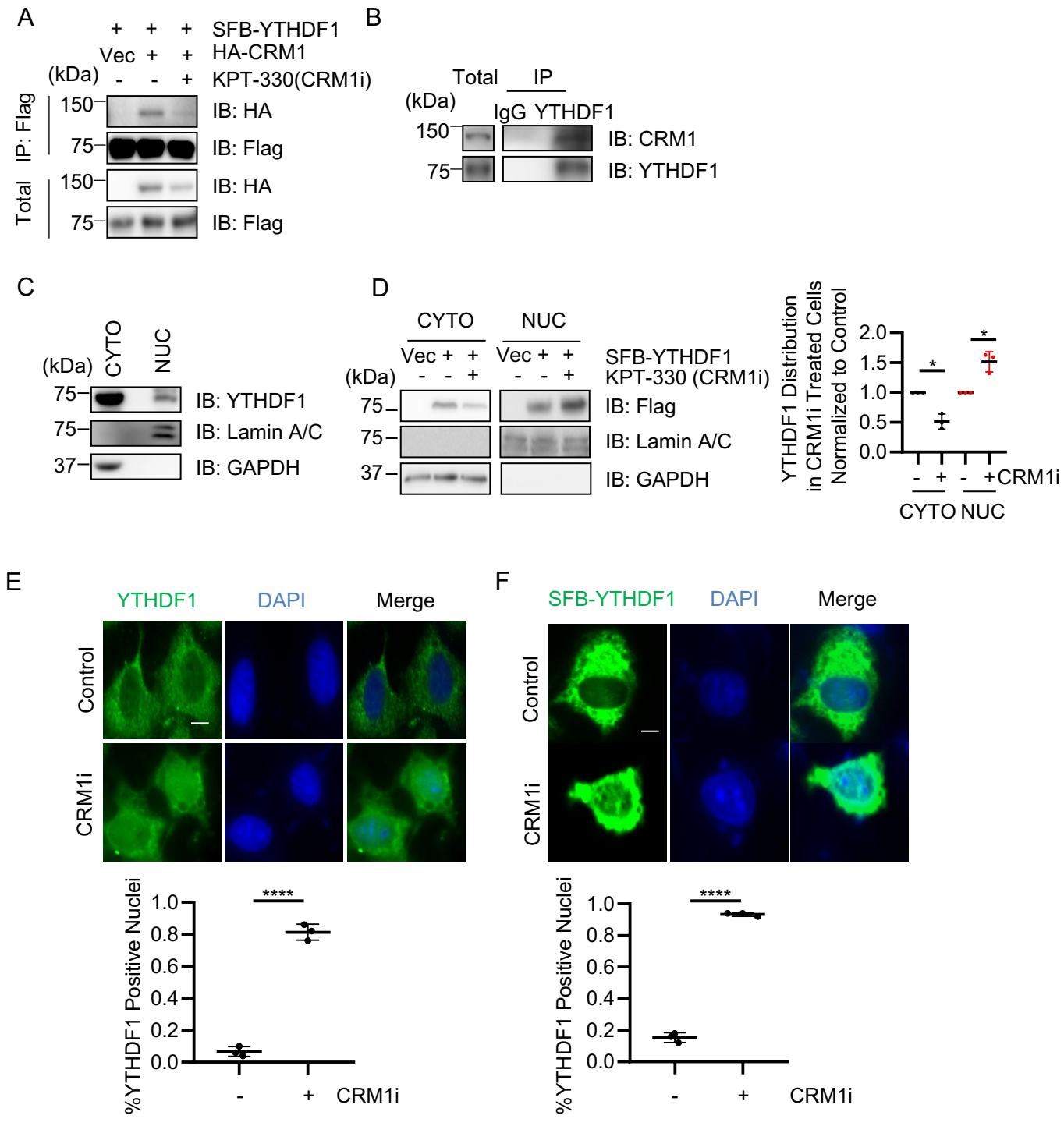
A
+ + + SFB-YTHDF1
Vec + + HA-CRM1
(kDa) - - + KPT-330(CRM1i)
IP: Flag
150
IB: HA
75
IB: Flag
Total
150
IB: HA
75
IB: Flag
B
Total
IP
(kDa)
IgG YTHDF1
150
IB: CRM1
75
IB: YTHDF1
C
(kDa) CYTO NUC
75
IB: YTHDF1
75
IB: Lamin A/C
37
IB: GAPDH
D
CYTO
NUC
Vec + + Vec + +
(kDa) - - + - - +
SFB-YTHDF1
KPT-330 (CRM1i)
75
IB: Flag
75
IB: Lamin A/C
37
IB: GAPDH
YTHDF1 Distribution in CRM1i Treated Cells Normalized to Control
2.0
1.5
1.0
0.5
0.0
- + - + CRM1i
CYTO NUC
E
YTHDF1
DAPI
Merge
Control
CRM1i
%YTHDF1 Positive Nuclei
1.0
0.8
0.6
0.4
0.2
0.0
****
- + CRM1i
F
SFB-YTHDF1
DAPI
Merge
Control
CRM1i
%YTHDF1 Positive Nuclei
1.0
0.8
0.6
0.4
0.2
0.0
****
- + CRM1i

Fig. 2

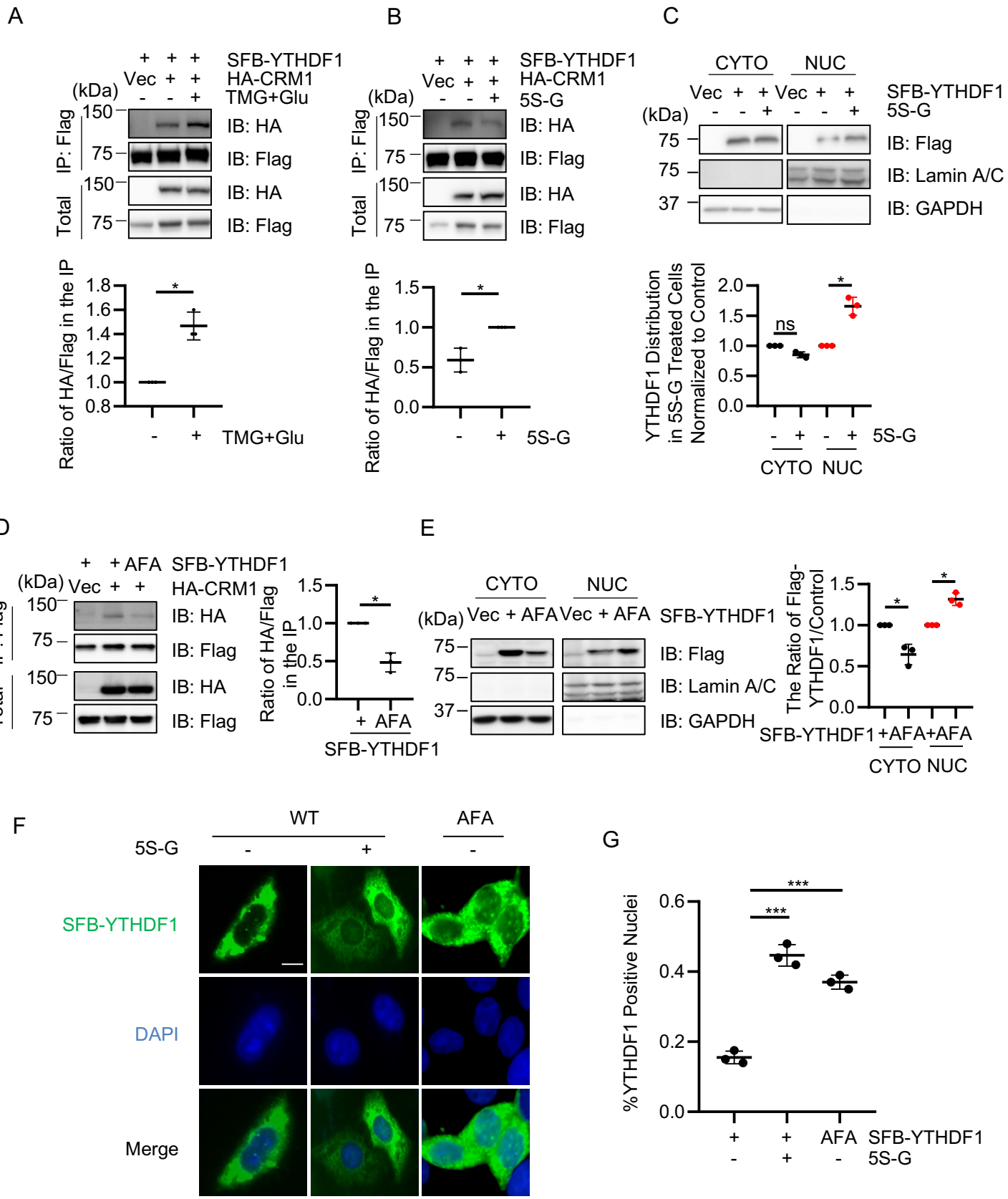
A
B
C
SFB-YTHDF1
HA-CRM1
TMG+Glu
5S-G
Vec
(kDa)
IP: Flag
Total
IB: HA
IB: Flag
Ratio of HA/Flag in the IP
CYTO
NUC
IB: Lamin A/C
IB: GAPDH
YTHDF1 Distribution in 5S-G Treated Cells Normalized to Control
ns
D
E
AFA
The Ratio of Flag-YTHDF1/Control
F
WT
AFA
SFB-YTHDF1
DAPI
Merge
G
%YTHDF1 Positive Nuclei

Fig. 3

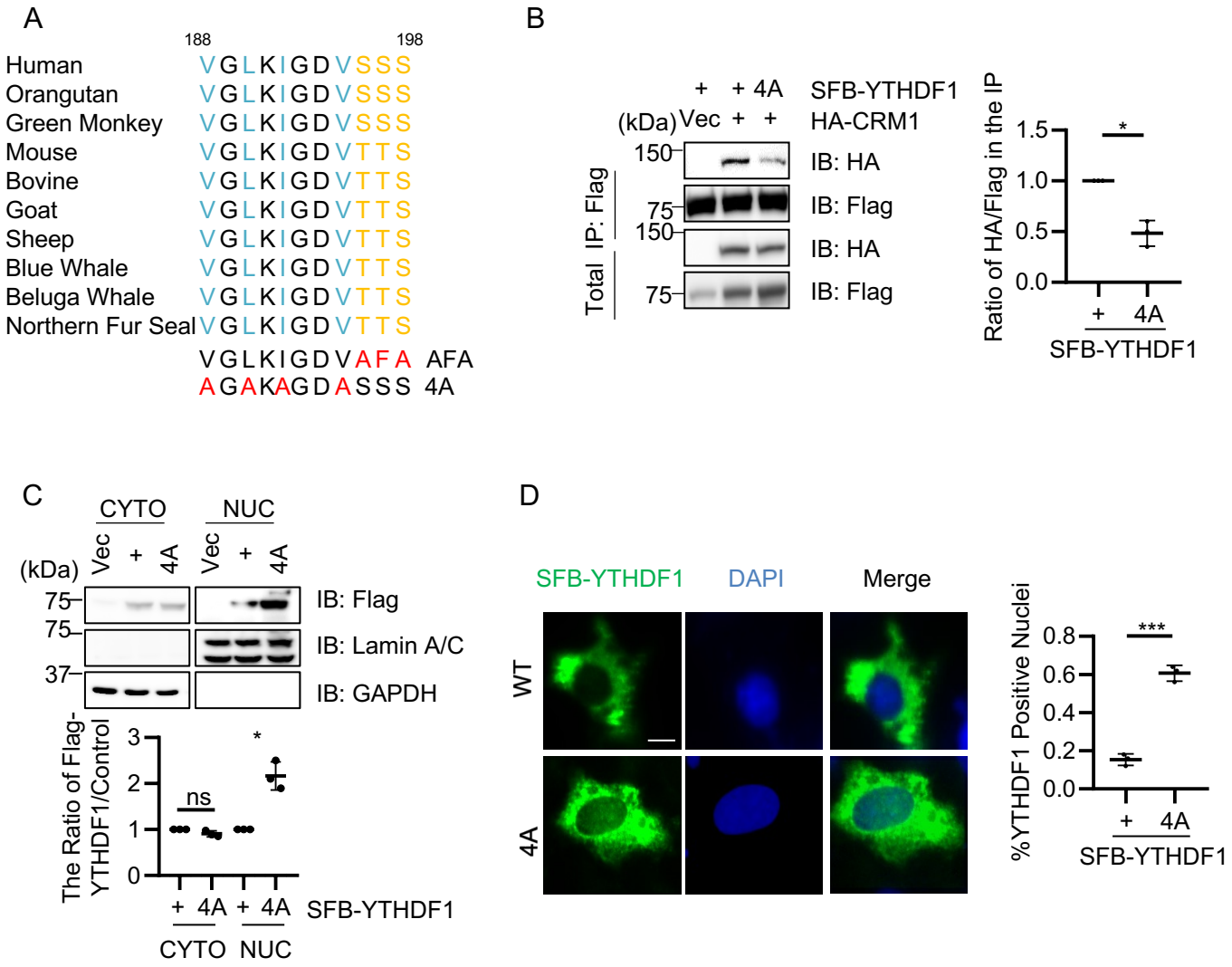
A
188
198
Human VGLKIGDVSSS
Orangutan VGLKIGDVSSS
Green Monkey VGLKIGDVSSS
Mouse VGLKIGDVTTS
Bovine VGLKIGDVTTS
Goat VGLKIGDVTTS
Sheep VGLKIGDVTTS
Blue Whale VGLKIGDVTTS
Beluga Whale VGLKIGDVTTS
Northern Fur Seal VGLKIGDVTTS
VGLKIGDVAFA AFA
AGAKAGDASSS 4A
B
+ + 4A SFB-YTHDF1
(kDa) Vec + + HA-CRM1
150
IB: HA
IP: Flag
75
IB: Flag
Total
150
IB: HA
75
IB: Flag
Ratio of HA/Flag in the IP
1.5
1.0
0.5
0.0
*
+ 4A
SFB-YTHDF1
C
CYTO
NUC
(kDa) Vec + 4A Vec + 4A
75
IB: Flag
75
IB: Lamin A/C
37
IB: GAPDH
The Ratio of Flag-YTHDF1/Control
3
2
1
0
ns
*
+ 4A + 4A SFB-YTHDF1
CYTO NUC
D
SFB-YTHDF1
DAPI
Merge
WT
4A
%YTHDF1 Positive Nuclei
0.8
0.6
0.4
0.2
0.0
***
+ 4A
SFB-YTHDF1

Fig. 4

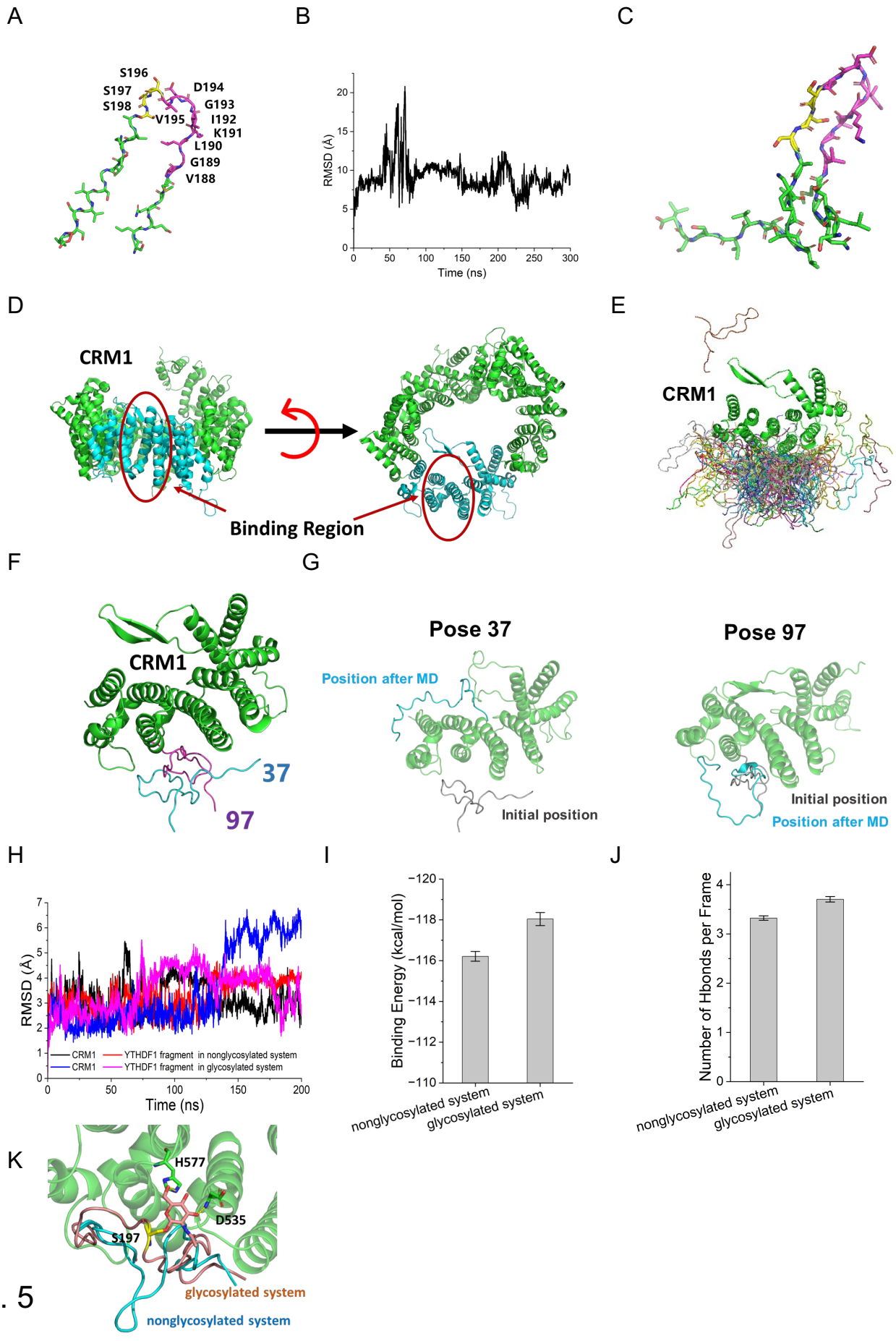
A
S196
S197
S198
D194
G193
V195
I192
K191
L190
G189
V188
B
RMSD (Å)
Time (ns)
C
D
CRM1
Binding Region
E
CRM1
F
CRM1
37
97
G
Pose 37
Position after MD
Initial position
Pose 97
Initial position
Position after MD
H
RMSD (Å)
CRM1
YTHDF1 fragment in nonglycosylated system
CRM1
YTHDF1 fragment in glycosylated system
Time (ns)
I
Binding Energy (kcal/mol)
nonglycosylated system
glycosylated system
J
Number of Hbonds per Frame
nonglycosylated system
glycosylated system
K
H577
D535
S197
glycosylated system
nonglycosylated system

Fig. 5

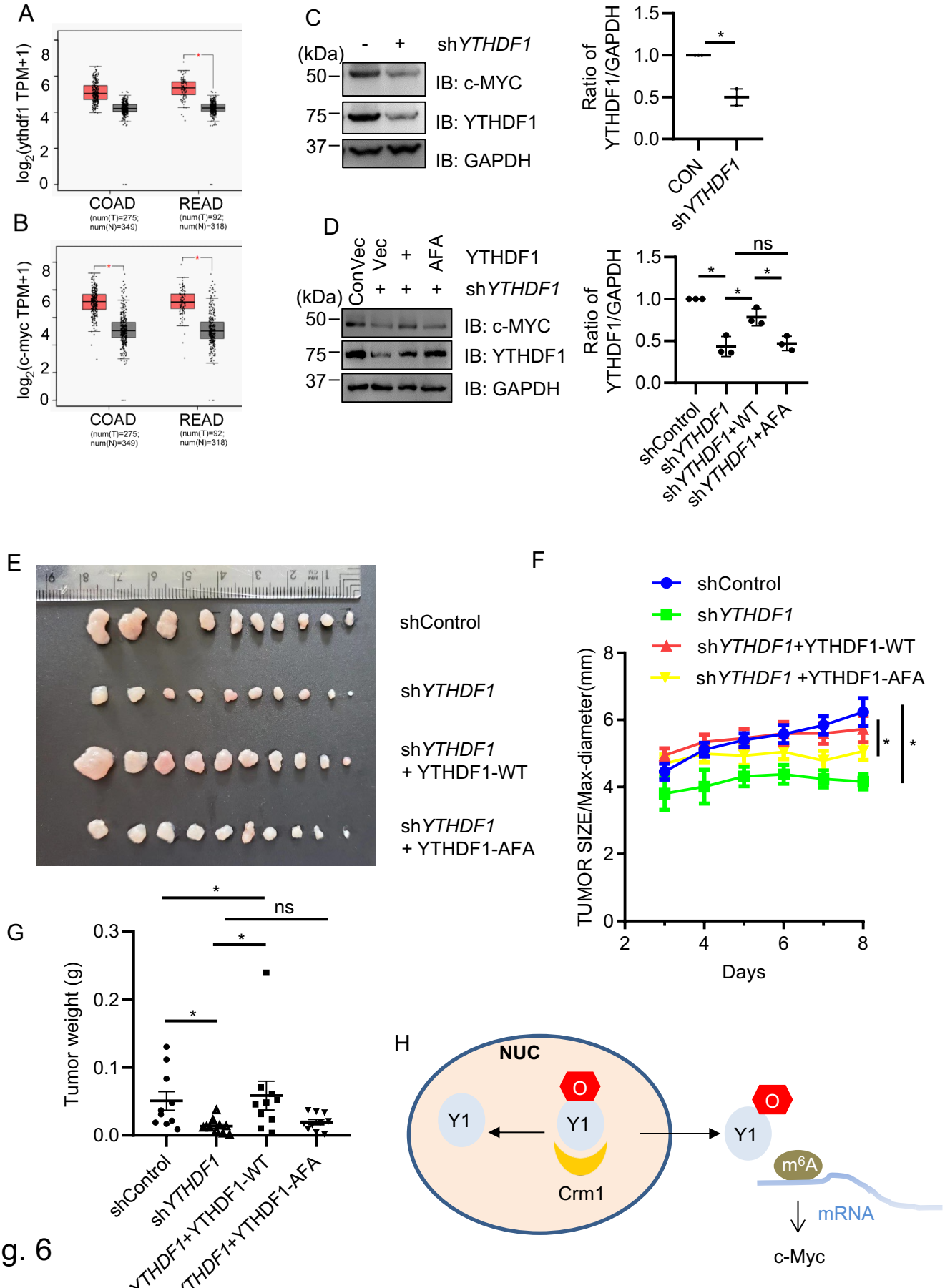
A
log2(ythdf1 TPM+1)
COAD
READ
(num(T)=275; num(N)=349)
(num(T)=92; num(N)=318)
B
log2(c-myc TPM+1)
C
(kDa)
shYTHDF1
IB: c-MYC
IB: YTHDF1
IB: GAPDH
Ratio of YTHDF1/GAPDH
CON
shYTHDF1
D
ConVec
Vec
AFA
YTHDF1
shYTHDF1
shControl
shYTHDF1+WT
shYTHDF1+AFA
ns
E
shControl
shYTHDF1
shYTHDF1 + YTHDF1-WT
shYTHDF1 + YTHDF1-AFA
F
shYTHDF1+YTHDF1-WT
shYTHDF1 +YTHDF1-AFA
TUMOR SIZE/Max-diameter(mm)
Days
G
Tumor weight (g)
H
NUC
Y1
O
Crm1
m6A
mRNA
c-Myc

Fig. 6